PHYSICAL REVIEW B VOLUME 36, NUMBER 18 15 DECEMBER 1987-II

Theory of the P_b center at the <111> Si/SiO$_2$ interface

Arthur H. Edwards
Electronic Technology and Devices Laboratory, U.S. Army Laboratory Command, Department of the Army, Fort Monmouth, New Jersey 07703-5000

(Received 22 May 1987)

We present a series of semiempirical calculations on threefold-coordinated silicon at the ⟨111⟩ Si/SiO$_2$ interface. These were performed on finite clusters of atoms with use of hydrogen terminators in an unrestricted Hartree-Fock formalism wherein we include lattice relaxations. We have calculated defect electrical levels as well as ESR hyperfine parameters. The agreement with Brower's principal hyperfine data is excellent. On the strength of this agreement, we assign the superhyperfine shoulders to spin density on three second-nearest-neighbor silicon atoms in the crystalline silicon. Our agreement with electrical data is good; we obtain a positive U of between 0.3 and 0.6 eV, depending upon the method of calculation. Finally, we predict the existence of a spin-dependent deep-level transient-spectroscopy signal at high pressure.

I. INTRODUCTION

Since the advent of metal-oxide-semiconductor (MOS) technology, it has been clear that most of the important phenomena in field-effect transistors occur at the interface between the semiconducting silicon and the insulating silicon dioxide. Specifically, the presence of electronic states localized at this interface and within the silicon band gap, called interface states, can alter a transistor's switching characteristics (both the position and abruptness of the threshold for current). Interface states have been studied intensely over the past twenty years. From this work a very rich picture of at least one class of interface states has emerged. The threefold-coordinated silicon at the ⟨111⟩ Si/SiO$_2$ interface, termed the P_b center,[1] is sufficiently well characterized experimentally, so that careful theoretical study is warranted.

In this paper we describe a molecular-orbital study of the P_b center.[2] Using semiempirical methods, we have performed total-energy calculations that include lattice relaxations for three charge states of this defect: $+1e$, 0, and $-1e$. We performed these calculations on finite clusters of atoms, and we studied the effects of cluster size. Our results are entirely in agreement with Brower's spin-resonance experiments[3] and, in fact, illuminate some of the details of his hyperfine data. We have also made estimates of the positions of the $(+/0)$ and $(0/-)$ gap levels and have obtained good semiquantitative agreement with the deep-level transient spectroscopy (DLTS) results of Johnson *et al.*[4]

The balance of this paper is organized as follows: In Sec. II, we give an outline of the experimental work on interface states in general, and on the P_b center in particular. In Sec. III, we discuss previous calculations. We also discuss our theoretical techniques, though briefly, as these have been discussed at length elsewhere.[5-7] We present our calculations in Sec. IV, and we conclude in Sec. V.

II. EXPERIMENTAL BACKGROUND

A. Electrical measurements

Interface states were first observed, albeit indirectly, in nonideal electrical characteristics in MOS capacitors. A compilation of some early results appears in Fig. 1(a) (Ref. 8). These data are derived from conductance-voltage[9] and capacitance-voltage[10] measurements. While data for both ⟨100⟩ and ⟨111⟩ interfaces are presented, in this paper we will only discuss the ⟨111⟩ interface, leaving the ⟨100⟩ for future publications. At first glance, the various sets of data appear to agree, and to follow the form suggested by the solid curve. However, Gray and Brown[11] (open circles) obtained peaks close to the band edges, while Kuhn[12] (×'s) observed richer structure than the U-shaped function assumed by White and Cricchi.[8] While some of these differences may be artifacts of special techniques (Gray and Brown, for instance, used a temperature-capacitance technique), recent experiments show that the total number of interface states, as well as the details of the spectroscopic dependence of the interface state density, depends strongly on sample preparation. Through careful processing, involving a high-temperature (1000 °C) post-oxidation anneal, as well as a low-temperature (450 °C) post-metallization anneal (or a 450 °C anneal in H$_2$ if there is no metal gate), the total density of interface states can be reduced to $\sim 10^{10}$ cm^{-2}. In this case, the spectrum of interface states *is* a rather featureless, U-shaped continuum that stretches across the silicon band gap with large values at either band edge. On the other hand, a process involving a high-temperature dry O$_2$ oxidation, but excluding both of the above-mentioned annealing steps, can produce total interface state densities in excess of 10^{12} cm^{-2}. In this case the interface state spectrum is altered dramatically in that two peaks are superimposed on the U-shaped background, as shown in Fig. 1(b). These data

**Work of the U. S. Government
Not subject to U. S. copyright**

were obtained by Johnson *et al.*[4] using deep-level transient spectroscopy (DLTS).[13] Other groups have reproduced these results using both quasistatic and low-frequency *C-V* methods.[14,15] These two peaks are directly related to the P_b center.

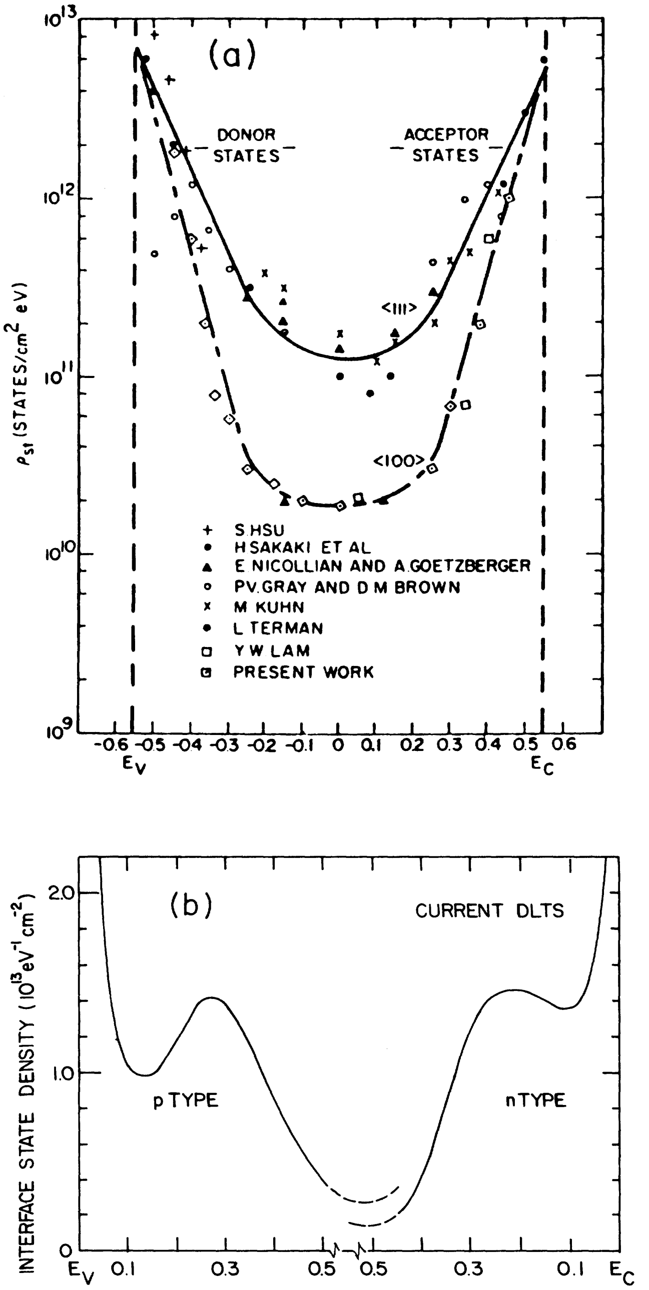

FIG. 1. Interface state spectra for two different cases of device processing. (a) All oxides have been annealed after metalization (from Ref. 8), (b) no postmetalization anneal (from Ref. 4).

B. Electron-spin resonance

While electrical measurements give insight into the spectral dependence of the density of interface states, other techniques are sensitive to the chemical nature of the interfacial defects that give rise to the observed electrical activity. Electron-spin resonance (ESR) is possibly the most important tool for obtaining detailed microscopic information about localized, paramagnetic defects in solids.[16] The earliest ESR experiments on oxidized silicon with no metal gate revealed all the important spectroscopic features.[1,17] That is to say, three peaks, labeled P_a, P_b, and P_c, were observed, two of which, P_b and P_c, showed strong dependence on the orientation of the crystalline substrate with respect to the applied magnetic field. Furthermore, etch-back experiments revealed that the P_b signal peaked very close to the Si/SiO$_2$ interface. In hindsight then, it is surprising that the P_b signal was attributed to a dangling silicon orbital in the SiO network.[1]

The MOS system was carefully reexamined by Poindexter and Caplan.[18] By comparing the *g* tensors of P_a, P_b, and P_c to the literature of defects in crystalline silicon, they were able to identify P_a as the donor electron residing in phosphorus doped substrates, and P_c as Fe^0, also in the bulk silicon. The anisotropy of the P_b *g* tensor combined with the absence of the P_b signal in unoxidized silicon led them to identify the P_b center as a singly occupied dangling silicon orbital at the Si/SiO$_2$ interface. We should point out that the same fabrication technique that gave rise to the two peaks in the density of interface states also maximized the observed density of P_b centers.

Recently, Brower observed the ^{29}Si hyperfine spectrum associated with the P_b center on the ⟨111⟩ interface.[3] His results are shown in Fig. 2. While we note that there are at least two sets of hyperfine interactions [as seen in Fig. 2(a)], Brower only analyzed the strong hyperfine lines. His analysis gives strong support to the Poindexter model. First, the ratio of the total intensity of the strong hyperfine interaction to the total intensity of the central ESR line (0.03) is consistent with the natural abundance of ^{29}Si (0.047), and not with the natural abundance of any other spin-$\frac{1}{2}$ species known to be present in the sample. Second, the magnitude of the hyperfine splitting can be directly related to the defect wave function through the relations[19]

$$A_{\parallel}=a+2b\ , \tag{1}$$

$$A_{\perp}=a-b\ , \tag{2}$$

where

$$a=\frac{8\pi}{3}gg_n\mu\mu_n\,|\psi_s(0)|^2\ , \tag{3}$$

$$b=\tfrac{2}{5}gg_n\mu\mu_n\langle\psi_p\,|\,r^{-3}\,|\,\psi_p\rangle\ . \tag{4}$$

In Eqs. (3) and (4), g and g_n are the g factors of the free electron and the magnetic nucleus, respectively, while μ and μ_n are the associated magnetons. ψ_s and ψ_p are the s and p components of the defect wave function (we are ignoring all higher angular momentum components). If

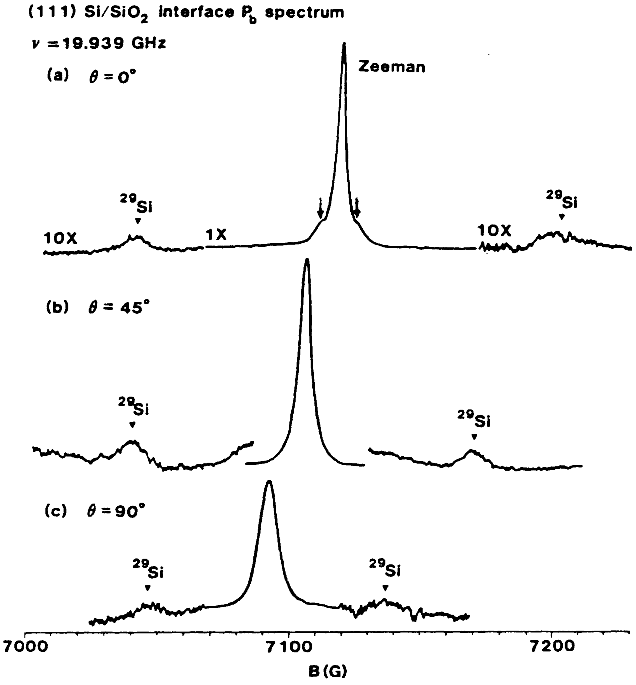

FIG. 2. ESR spectra of the P_b center observed from ⟨111⟩ Si/SiO$_2$ interface. The magnet is rotated in a ⟨112⟩ plane; θ is the angle between the ⟨111⟩ direction and the direction of B. ($\theta=90°$ corresponds to B parallel to the ⟨110⟩ direction.) Figure taken from Ref. 3.

the defect wave function is expressed as a molecular orbital of the form

$$\psi=\sum_i \eta_i(\alpha_i\,|\,s_i\rangle+\beta_i\,|\,p_i\rangle)\ , \tag{5}$$

where i indexes atomic sites, then the observed splittings imply that 80% of the unpaired spin is located on a single silicon atom, and that this localized spin density has 12% s character and 88% p character, with the p lobe pointing in the ⟨111⟩ direction.

We have recounted the hyperfine results in detail, because they are the most convincing experimental data, and because we can relate them to our calculated wave functions through Eqs. (1)–(4). Below, we will discuss our interpretation of both the strong and weak hyperfine interactions.[20]

C. Field-dependent ESR

Several groups have combined ESR with various electrical techniques for altering the position of the Fermi level in the band gap.[4,14,21] By monitoring the strength of the P_b signal as a function of Fermi level, it was found that the two peaks in the density of interface states correspond well with the (+/0) and the (0/−) transitions of the P_b center. That is to say, if the Fermi level is within 0.3 eV of the valence-band edge, then the defect level is unoccupied and gives rise to no spin signal. If the Fermi level is between 0.3 and 0.9 eV above the valence band, then the P_b center is singly occupied, and the normal spin signal is observed. Above 0.9 eV the defect becomes doubly occupied and diamagnetic. This result clearly shows that the P_b center is a positive-U system with a 0.6-eV effective e-e correlation energy.

To summarize, the peaks in the density of interface states observed in specially fabricated samples have been correlated with the (+/0) and (0/−) transitions for a dangling orbital on a trivalent silicon atom at the Si/SiO$_2$ interface. Any theoretical treatment of this defect should address both the level positions and the hyperfine data.

III. THEORETICAL BACKGROUND

Several groups have studied the dangling silicon orbital. The calculations can be conveniently split into two categories: Green's-function techniques applied to infinite systems, and molecular-orbital techniques applied to finite clusters of atoms.

A. Green's-function calculations

The earliest and simplest Green's-function calculations on the interface and its defects, by Laughlin *et al.*,[22] were non-self-consistent, wherein the bulk silicon and bulk SiO$_2$ were represented by Bethe lattices connected through a single interface bond. The dangling bond was generated by removing the oxide Bethe lattice. (Note that this calculation might be more representative of the dangling bond in a-Si.) The important predictions were that the perfect interface would have no gap states, while the dangling orbital would yield a state in the gap. However, the lack of self-consistency, and hence of effects of changes in electron occupation, combined with the absence of defect-lattice interaction, limit the usefulness of these calculations severely.

A far more interesting study of the same system (a single trivalent silicon atom attached to three silicon Bethe lattices) was performed by Ngai and White.[23] By using Harrison's[24] universal expressions for the distance-dependent, tight-binding parameters, they modeled the effect of relaxation of the defect atom. Furthermore, by using a generalized version of Harrison's bond-orbital approximation,[25] in which lattice relaxation and charge state effects are treated simultaneously, these investigators were able to capture much of the physics revealed in other more complex calculations.

Two other non-self-consistent calculations have addressed the two-dimensional character of the problem. Sakurai and Sugano[26] considered only the ⟨111⟩ Si/SiO$_2$ interface while Carrico *et al.*[27] considered ⟨111⟩ as well as ⟨110⟩ and ⟨100⟩. Both of these groups used tight-binding Green's-function techniques, and both represented the oxide with Bethe lattices. If one considers only the results for the ⟨111⟩ dangling bond, then these calculations add no new insight. Rather, they demonstrate that, within the simple tight-binding scheme, the results were not altered significantly by considering a surface rather than a single atom. Both of these papers have other features to recommend them. By considering the three differently oriented surfaces, Carrico *et al.* showed that the ⟨111⟩ dangling bond and the ⟨110⟩ dangling bond were essentially the same, which is in agreement with spin resonance.[18] Further, the particular dangling bond considered at the ⟨100⟩ interface (on a silicon atom attached to two silicons and one oxygen) does not give rise to a gap state in their calculations. This is in agreement with other calculations.[22,28] The value of the Sakurai-Sugano calculations lies in their exploration of the effects of strained bonds and impurities at the interface.

Recently, two self-consistent-model calculations have appeared on the dangling silicon orbital.[29,30] Neither of these calculations includes lattice relaxation effects, but both predict two levels in the silicon gap separated by 0.5 eV.

Finally, we note that two calculations have been performed on the dangling bond in crystalline silicon using Green's-function local-density techniques.[31–33] The most recent,[32] in which total-energy surfaces as a function of atomic position were calculated for the positive, neutral, and negative charge states, predicts that this system has an Anderson negative U.[34] If true, this would imply that the dangling bond is always diamagnetic—contrary to experiment. We will discuss this calculation in Sec. IV.

B. Cluster calculations

Several calculations have appeared on finite clusters of atoms used to represent the dangling bond. Redondo *et al.* performed *ab initio*, generalized valence-bond (GVB) calculations on the Si$_4$H$_9$ cluster.[35,36] They performed calculations for positive, negative, and neutral charge states and found the equilibrium geometry in each. In fact, as we will show in Sec. III C, we obtain very similar results when we consider the same size cluster, even though we are using much simpler methods.

Very recently, Cook and White[37] have performed a set of calculations using scattered-wave X-α techniques applied to very large clusters. Because the scattered-wave technique does not yield reliable total energies, they considered only two geometries: the ideal tetrahedral configuration and an equilibrium geometry we discuss below. The strength of these calculations lies in the quality of the numerical wave functions with which they calculate the hyperfine coupling constants from first principles. The agreement with experiment is very good, considering the sensitivity of these observables to very small changes in the calculated defect wave function. This sensitivity is discussed in Sec. IV.

C. Present theoretical technique

In our calculations, we used a semiempirical LCAO molecular-orbital program, MOPN.[6] This is a spin-unrestricted version of MINDO/3 (modified intermediate neglect of differential overlap).[5] The most important features of the technique are the following.

(1) MINDO/3 is part of the family of neglect of differential overlap (NDO) approximations, i.e.,

$$\phi_{n_A}(r)\phi_{m_B}(r)dr=0,\quad n_A\neq m_B\ . \tag{6}$$

Here, A and B denote different atomic sites, and n_A and m_B denote the different sets of atomic quantum numbers associated with the functions $\phi_{n_A}(r)$ and $\phi_{m_B}(r)$. This approximation eliminates all three- and four-center integrals, and reduces the number of two-center integrals greatly.

(2) In MINDO/3 the remaining one- and two-center integrals are either evaluated using semiempirical formulas, or are fitted to experimental heats of formation, molecular geometries, dipole moments, and ionization potentials.

(3) This program includes software that optimizes the total energy with respect to chosen atomic coordinates.[38]

Because MOPN is self-consistent, we are able to consider several charge states. Further, it is a total-energy technique, so that electron-lattice interactions are well represented. Finally, because it is spin unrestricted, we can calculate a spin-density matrix that is summed over all occupied states. That is to say, we can go beyond simple one-electron theory wherein we consider only the defect molecular orbital to estimate ESR parameters. As we will show in Sec. IV, this will be very important in understanding some of the details of the hyperfine interaction.

In our calculation of hyperfine matrices we use a more general form of Eqs. (1)–(4). For a single Slater determinant in the unrestricted Hartree-Fock formalism, the hyperfine dyadic for magnetic nucleus k is[39]

$$A_{ij}=gg_n\mu\mu_n\left[\sum_{\eta}\langle\phi_\eta^\alpha|H_{\text{hyp}}|\phi_\eta^\alpha\rangle-\sum_{\eta}\langle\phi_\eta^\beta|H_{\text{hyp}}|\phi_\eta^\beta\rangle\right]. \tag{7}$$

Here, $|\phi_\eta^{\beta(\alpha)}\rangle$ are the one-electron molecular orbitals, α and β are spin quantum numbers, and

$$H_{\text{hyp}}=\frac{8\pi}{3}\delta^3(r_k)+\frac{3r_{ki}r_{kj}-\delta_{ij}r_k^2}{r_k^5}\ . \tag{8}$$

In LCAO theory,

$$|\phi_\eta^\alpha\rangle=\sum_{n_A}C_{n_A}^{\eta\alpha}|n_A\rangle\ , \tag{9}$$

where A labels the atom and n_A indexes a set of atomic quantum numbers (s,p_x,p_y,p_z). In the atomic basis, Eq. (7) becomes

$$A_{ij}=gg_n\mu\mu_n\sum_{\substack{n_A\\ m_A}}S_{n_Am_A}\langle n_A|H_{\text{hyp}}|m_A\rangle\ , \tag{10}$$

where $S_{n_Am_B}$ is the net spin-density matrix, i.e.,

$$S_{n_Am_A}=\sum_{\eta}C_{n_A}^{\eta\alpha}C_{m_A}^{\eta\alpha}-\sum_{\eta}C_{n_A}^{\eta\beta}C_{m_A}^{\eta\beta} \tag{11}$$

(η is summed over occupied states), and where we have used the NDO approximation. Hence, the hyperfine dyadic on a single atom can be written

$$\begin{bmatrix} S_{ss}a+[S_{xx}-\frac{1}{2}(S_{yy}+S_{zz})]2b & 3S_{xy}b & 3S_{xz}b \\ 3S_{yx}b & S_{ss}a+[S_{yy}-\frac{1}{2}(S_{xx}+S_{zz})]2b & 3S_{yz}b \\ 3S_{zx}b & 3S_{zy}b & S_{ss}a+[S_{zz}-\frac{1}{2}(S_{xx}+S_{yy})]2b \end{bmatrix}, \qquad (12)$$

where a and b are given in Eqs. (3) and (4). Our semiempirical molecular-orbital technique precludes calculation of these matrix elements directly, as its valence-only basis set is not orthogonalized to an appropriate set of core orbitals. Instead, we use our calculated spin-density matrix, combined with *ab initio* Hartree-Fock values[19] for a and b, to calculate theoretically predicted hyperfine dyadics.

We have made limited use of GAUSSIAN 82,[40] an *ab initio* molecular-orbital program that allows the use of a variety of basis sets in both restricted and unrestricted Hartree-Fock formalisms.

IV. CALCULATIONS AND DISCUSSION

We have applied the techniques discussed in Sec. III to the atomic clusters shown in Fig. 3. With the exception of cluster 1, we have not shown the hydrogen atoms used to complete the fourfold coordination of all silicon atoms with the exception of the defect silicon atom, solid circles in Fig. 3. While there are other more sophisticated methods of cluster termination,[41,42] the hydrogen atoms achieve the principal goal of removing the surface-state energy levels from the neighborhood of the defect energy level. Thus these levels do not admix, and there is no appreciable spin density appearing at the surface—in agreement with experiment. We used these several clusters to study the convergence of the various calculated results—ESR parameters, equilibrium geometries, and energy levels—as a function of cluster size. For each of three charge states (+ 1,0, − 1) we calculated the total energy as a function of defect relaxation. Except where noted, we allowed only the defect atom to relax.

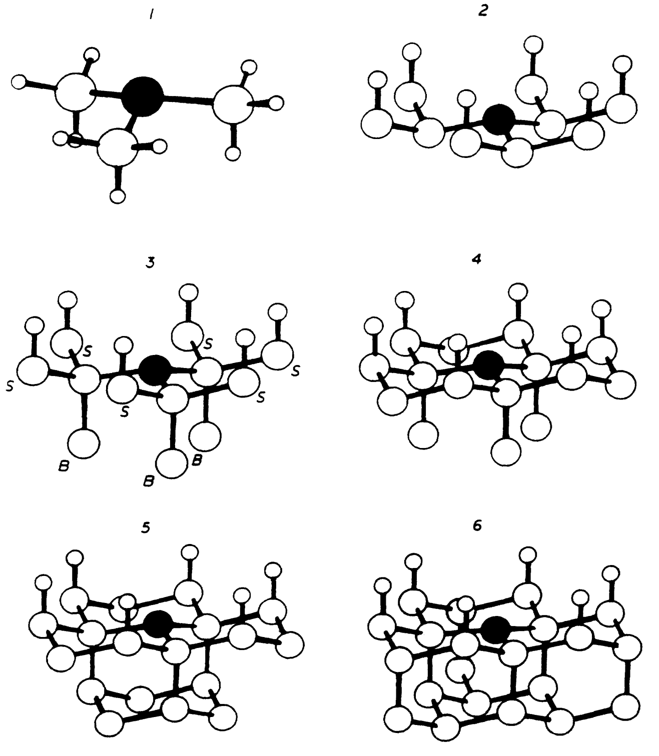

FIG. 3. Atomic clusters used in present calculations. In clusters 2–6, we do not show hydrogen terminators. The defect atom is shown by a solid circle.

A. Si_4H_9

While the calculations on larger clusters reveal more of the physics of the P_b center, for the sake of calibration, we compare our semiempirical results with other *ab initio* results for cluster 1. Redondo *et al.*[35,36] studied this cluster as part of a larger investigation of the ⟨111⟩ silicon surface. We have studied it using both MOPN and GAUSSIAN 82. In our *ab initio* study we used several basis sets—STO-3G and STO-6G (minimal basis sets wherein three and six Gaussian functions, respectively, are used to represent each Slater orbital), STO-3G* (a basis set that includes $3d$ silicon atomic orbitals), and 3-21G [a split-valence basis set in which the valence orbitals ($3s$ and $3p$ in the case of silicon, $1s$ in the case of hydrogen) are represented by two Slater-type orbitals labeled inner and outer]. Table I is a compilation of equilibrium geometries and defect orbital compositions obtained in these *ab initio* unrestricted calculations. For comparison, we have included our semiempirical results as well as the GVB results of Redondo *et al.* While we have allowed the defect atom complete freedom, the relaxation is essentially perpendicular to the ⟨111⟩ silicon surface. This was true for all the clusters we considered. Here, as in other cases, there is a rather broad distribution in the *ab initio* results, depending upon basis set and calculation scheme. Note that in all cases the defect atom moves toward the plane of its three nearest neighbors in both the neutral and positive charge states, while moving away in the negative charge state.

As a special case, we have calculated an equilibrium geometry for a completely unconstrained cluster. In this case, the defect atom is virtually *in* the plane of its three silicon neighbors. This is expected in the case of completely covalent bonds. The pyramidal geometry in all other calculations is thus a result of the constraints imposed by the host silicon crystal.

We now turn to the wave-function composition. There is no unique scheme for determining the orbital composition except when the atomic orbitals are nono-

TABLE I. Equilibrium geometries for the $(+,0,-)$ charge states, and defect orbital composition for the (0) charge state for various *ab initio* techniques and for MOPN applied to Si$_4$H$_9$. $D_{(+,0,-)}$ (in Å) measures the motion along the $\langle 111 \rangle$ direction away from the ideal tetrahedral position of the defect atom. ρ_{tot} is the total defect wave-function density on the defect atom, and ρ_p is the associated p density on the defect atom.

	STO-3G	STO-6G	STO-3G*	3-21G	Ref. 36	MOPN
D_+	-0.42	-0.42	-0.43	-0.33	-0.38	-0.46
D_0	-0.16	-0.16	-0.16	-0.003	-0.08	-0.2
D_-	0.19	0.19	0.15	0.34	0.17	0.13
ρ_{tot}	0.73	0.74			0.93	0.74
ρ_p/ρ_{tot}	0.98	0.98			0.93	0.94

verlapping, as is formally the case in any NDO approximation. For our *ab initio* calculations, we used

$$|\langle \phi_D | \phi_\eta^\alpha \rangle|^2 = \sum_{\substack{n_A, \\ n_B}} C_{n_A}^{\eta\alpha} C_{m_B}^{\eta\alpha} \langle \phi_D | n_A \rangle \langle m_B | \phi_D \rangle \ . \quad (13)$$

In all of our calculations, there is strong localization of the highest occupied molecular orbital on the defect atom ($\sim$73%). This is smaller than the quoted GVB value (93%), though the method of decomposition is unstated in Ref. 36. The ratio of the s and p contributions on the defect atom is virtually independent of molecular-orbital technique. The results presented in Table I lend support to our use of semiempirical techniques in all calculations described in the balance of this paper.

B. The paramagnetic P_b center

We gain an appreciation for the physics of the paramagnetic charge state of the P_b center by considering the effects of cluster size. In Fig. 4, we show the equilibrium geometry for clusters 1–6. In this figure, D_t denotes the distance between the defect atom and the plane containing its three nearest-neighbor silicon atoms for the ideal tetrahedral configuration, while D' is the same distance in the equilibrium configuration ($D'=D_t-D$, where D is defined in Table I). Note that in all cases, the equilibrium position for the P_b atom lies below the ideal tetrahedral position. This should be expected, as it allows the nearest-neighbor bonds to strengthen.[43] The decrease in total energy is due principally to changes in the Hamiltonian matrix elements. That is to say, the changes in the bond-order matrix as a function of position are at least an order of magnitude too small to account for the change in energy. We note that the equilibrium geometry changes noticeably with the addition of the three bulk silicon atoms in cluster 3.

In Fig. 4, we also show the spin density on the central atom as a function of cluster size. Several features bear comment. First, the value for cluster 1, 0.94, is larger than the total defect wave-function amplitude on the defect atom, 0.74. This difference reflects the spin polarization of the valence-band states.[44] Second, we note the importance of the three second-nearest-neighbor bulk silicon atoms, labeled **B** in cluster 3, Fig. 3. Their addition lowers the spin density on the defect atom by 0.13, bringing it close to Brower's experimental estimate. The surplus spin density resides on these three silicon atoms. We believe this transfer of spin density is not an artifact, as it persists in all clusters larger than cluster 3. It is also observed in Cook's X-α calculations on a cluster closely related to our cluster 6.[37] Furthermore, our hyperfine estimates, discussed below, indicate that it accounts for the weak hyperfine shoulders seen in Fig. 2(a).

Using the analysis outlined in Sec. III, we have calculated hyperfine dyadics on the defect atom, its nearest-, and second-nearest-neighbors from our calculations on cluster 5 in the minimum-energy configuration. The principal values of these dyadics are shown in Table II(a). These are to be compared with Brower's experimental values given in Table II(c). We consider the agreement between experiment and theory to be very good. Note that the only important hyperfine interactions are on the defect atom and its second nearest neighbors in the bulk. The predicted splitting on these second nearest neighbors is in good agreement with the observed superhyperfine shoulders evident in Brower's spectra [Fig. 2(a)]. We have also determined the directions of the principal axes of these dyadics. A_3 on the defect atom is 0.05° away from the $\langle 111 \rangle$ direction, while it is 1.62° away on the bulk second nearest neighbors.

For reasons discussed in Sec. III, Table II does not constitute a definitive theoretical confirmation of Poindexter's model of the P_b center, though it is entirely consistent with it. Furthermore, as mentioned above,

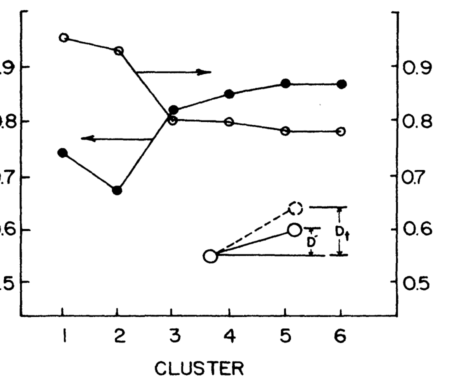

FIG. 4. Equilibrium geometry and spin density on the defect atom as a function of cluster size. D_t denotes the ideal tetrahedral distance between the defect atom and the plane of its three nearest-neighbor silicon atoms.

TABLE II. Principal values of hyperfine dyadics on various atom types for cluster 5. (a) Calculated in the equilibrium geometry for cluster 5; (b) calculated in the equilibrium geometry for cluster 2; (c) experiment (Ref. 3). All values in Gauss.

	A_1	A_2	A_3
	(a)		
Defect atom	123.9	123.9	179.2
Nearest neighbor	−0.71	2.31	3.55
Bulk second nearest neighbor	17.62	18.21	23.26
Surface second nearest neighbor	−1.24	−1.03	−1.02
	(b)		
Defect atom	96.5	96.5	157.2
Nearest neighbor	−3.99	−0.93	−0.72
Bulk second nearest neighbor	21.2	21.8	27.0
Surface second nearest neighbor	−2.86	−2.14	−1.87
	(c)		
Strong hyperfine	91.0	91.0	156.0
Superhyperfine			18.0

these results give a natural explanation for the weak hyperfine shoulders evident in Brower's ESR data. That the shoulders are significantly higher than the strong hyperfine peaks (note change in scale; hyperfine peaks are magnified ten times relative to the central peak) is consistent with a threefold increase in the probability that a magnetic nucleus will appear as one of three second-nearest-nearest-neighbor silicon atoms. The good agreement between our theoretical result and our estimate of the experimental superhyperfine splitting, combined with the absence of any other hyperfine interaction of appropriate magnitude in our calculation, is a strong argument that these shoulders indeed arise from the three bulk second-nearest-neighbor silicon atoms.

It is instructive to study the variation of these hyperfine parameters with the position of the defect atom. Table II(b) lists our values for cluster 5 with the defect atom in the equilibrium position for cluster 2. The agreement with experiment, while excellent, should not be considered definitive, for reasons stated above. Rather, it demonstrates the sensitivity of ESR to small changes in the defect environment. Differences of a few percent in spin density have given rise to very large differences, ~17%, in the predicted splittings.

We now turn our attention to the one-electron energy levels. Recall that in the frozen orbital approximation these correspond to ionization potentials, and that MINDO/3 has been parametrized to reproduce these accurately in molecules. If we have included enough silicon atoms to simulate bulk silicon, then we can estimate the position of the optical levels of the P_b center in the band gap.

In Fig. 5 we show, as a function of cluster size, the energy levels for the two highest occupied valence states. 58% of the wave-function density of the highest occupied valence state resides on the defect atom. Furthermore, as we will discuss below, this level is almost completely decoupled from the second highest orbital. For these reasons we identify the highest level as the defect level, and the second highest level as the top of the valence band. In Fig. 5, the circles indicate the defect energy levels with the defect atom in the same position, 0.26 Å below the ideal tetrahedral geometry (toward the back-bonded silicon atoms), so that they reflect only changes in the electronic structure as a function of cluster size. The squares indicate the same energy levels calculated in the equilibrium geometry for each cluster, and hence include electron-lattice effects.

For clusters 4, 5, and 6, the results are independent of cluster size, so that we consider them well converged. Note that the inclusion of surface rings in cluster 4 increases the energy of the top of the valence band by 0.32 eV. We believe this increase is due to delocalization of the highest valence-band wave function onto the third-nearest-neighbor surface ring atoms from the nearest-neighbor atoms. While delocalization is usually associated with decreased energy, in this case it is not, because it lowers the bonding character between the nearest- and second-nearest-neighbor silicon atoms.

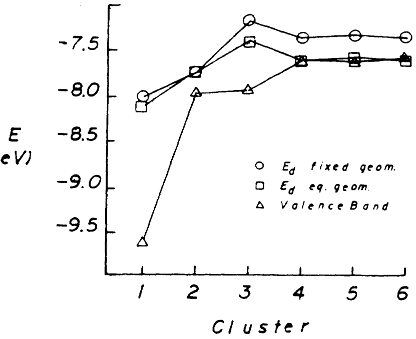

FIG. 5. Calculated one-electron energies corresponding to the valence-band edge and the defect orbital. These are shown as a function of cluster size.

For the largest clusters, when the electron-lattice interaction is included in the calculation, the defect level is degenerate with the top of the valence band, contrary to experiment. We believe this results from an underestimation of the defect atom relaxation. This is an obvious possibility in light of the results shown in Fig. 5. The more strongly relaxed defects (circles) have energy levels further away from the valence-band edge. Also, our results on the unconstrained cluster, wherein the P_b center is planar, emphasize the proclivity toward strong relaxation. Furthermore, as shown in Table III, MINDO/3 systematically overestimates silicon-silicon bond lengths, so that we would expect the predicted equilibrium position of the P_b atom to be too high, hence driving the energy too low. Finally, as we noted above, our predictions of the hyperfine parameters improved when we increased the relaxation.

In Fig. 6 we show the position with respect to the valence-band edge of the singly and doubly occupied defect states as a function of the relaxation below or above the tetrahedral configuration. (D has the same meaning as in Table I.) This figure shows clearly that the defect state energy increases as the defect atom moves closer to its nearest neighbors, while the top of the valence-band stays relatively constant. Ngai and White predicted this on the basis of increased p admixture and, hence, a larger diagonal matrix element on the defect atom.[23] We attribute this also to an antibonding interaction between the orbitals on the defect atom and the second-nearest-neighbor bulk silicon atoms, as well as a weak antibonding interaction between the defect atom and its nearest neighbors.

TABLE III. Equilibrium bond lengths for atomic clusters used to simulate crystalline silicon. $R_{\text{Si-Si}}(\text{expt}) = 2.35$ Å. All lengths are given in angstroms.

Si_5H_{12}	2.37
$Si_{17}H_{36}$	2.50

Figure 6 suggests the possibility of a spin-dependent DLTS signal.[45] If a restricted set of P_b centers is under significant compressive strain, then, as shown in Fig. 6, the one-electron levels will move in concert toward the valence-band as the equilibrium position of the defect atom moves toward the oxide. During a DLTS pulse that would normally depopulate the singly occupied level, these compressed centers, which in equilibrium would be doubly occupied, would be pulsed into their singly occupied state. Then, during the normal repopulation cycle, these special sites would be subject to a classic singlet-triplet bottleneck (the singlet or triplet state is formed by the electron on the defect and an electron in the conduction band), so that the capture rate would be altered dramatically during spin resonance.

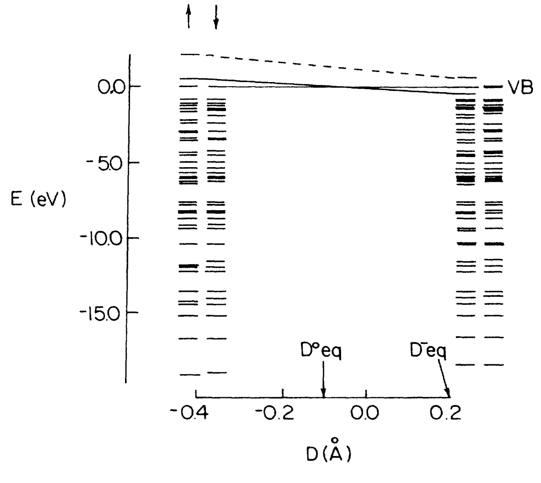

FIG. 6. One-electron energy levels for cluster 6 shown as a function of defect-atom position. D measures motion perpendicular to the interface ($D = 0$ indicates the ideal tetrahedral position). The dashed line is doubly occupied, and the solid line is singly occupied. The arrows indicate the spin states for the spin-unrestricted wave functions of the neutral charge state. $D_{\rm eq}^{0}$ and $D_{\rm eq}^{-}$ indicate the equilibrium geometries for the neutral and negative charge states, respectively.

Our prediction of the positions of the singly and doubly occupied levels as a function of strain can be tested experimentally. Using diamond anvils, some researchers have obtained hydrostatic pressures of 100 kbar.[46,47] Using a semiempirical equation for the bulk modulus of silicon, it can be shown that under this pressure the lattice constant changes by 4.8%.[48] Simple calculations on a compressed cluster indicate that the levels should move by ~0.17 eV. This should be observable in high-pressure *in situ* DLTS experiments. It is even conceivable that spin-dependent DLTS could be observed assuming a diamond anvil could be mounted in an ESR cavity.

C. Nonparamagnetic charge states

With the analysis of the neutral state of the P_b defect as a backdrop, the behavior of the positive and negative charge states of the P_b center can be understood easily. By removing an electron from an antibonding state, we

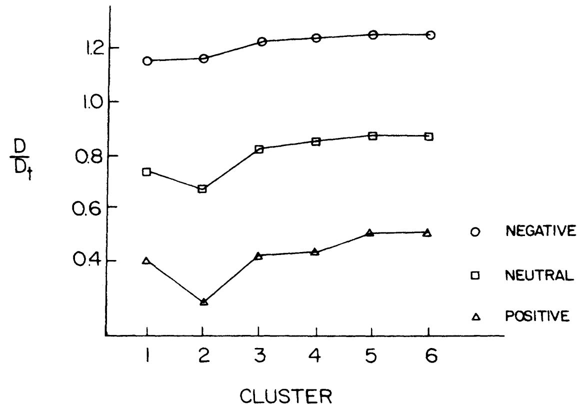

FIG. 7. Equilibrium geometry for the positive, neutral, and negative charge states as a function of cluster size. D' and D_t are the same as in Fig. 4.

would expect the overall bonding to increase, and the defect atom to seek an equilibrium configuration closer to its three nearest neighbors. Conversely, by adding an electron to the defect level, we would expect that the defect atom would move away from its nearest neighbors to lower the energy of the antibonding state. Both of these predictions turn out to be the case. In Fig. 7 we show the equilibrium position of the defect atom as a function of cluster size for the positive and negative charge states, respectively. We note that these changes in bondlength with respect to charge state have been used as a criterion for the character (bonding, nonbonding, or antibonding) of pertinent molecular orbitals.[49] On the basis of Fig. 7, then, we consider the defect orbital to be antibonding.

D. Correlation energy

We can use Fig. 6 to estimate the effective correlation energy for the P_b center. The arrows indicate the levels at equilibrium geometry. Using

$$U^{1\,\mathrm{el}}=(E_{\mathrm{def}}-E_{\mathrm{VB}})^{-}-(E_{\mathrm{def}}-E_{\mathrm{VB}})^{0}\ , \tag{14}$$

where E_{def} and E_{VB} are the energy levels of the highest and second-highest (valence-band) occupied molecular orbitals for the neutral (0) and negatively charged $(-)$ clusters, we estimate that the effective correlation energy is 0.6 eV. So, on the basis of these one-electron energy levels, we predict that the P_b defect is a normal, positive-U defect.

We have also estimated the correlation energy using total-energy calculations. We have used a double-cluster approach, involving a completely passivated cluster (cluster 5 with a seventh OH group attached to the defect atom), to calculate a theoretical electron affinity, ionization potential, and band gap. These were calculated by letting only the defect atom move, as in the defect calculations. We estimate the singly occupied level position with respect to the valence-band edge,

$$E_{\mathrm{def}}-E_{\mathrm{VB}}=(E_{\mathrm{def}}^{+}+E_{\mathrm{pass}}^{0})-(E_{\mathrm{def}}^{0}+E_{\mathrm{pass}}^{+})\ , \tag{15}$$

and the doubly occupied level with respect to the conduction-band edge,

$$E_{\mathrm{def}}-E_{\mathrm{CB}}=(E_{\mathrm{def}}^{-}+E_{\mathrm{pass}}^{0})-(E_{\mathrm{def}}^{0}+E_{\mathrm{pass}}^{-})\ . \tag{16}$$

Here, all energies are total energies, def refers to cluster 5, pass refers to the passivated cluster, and the $+$, 0, and $-$ superscripts refer to the charge state of the cluster. The band gap, 1.6 eV, is estimated from an excited triplet-state calculation performed on the neutral passivated cluster.[50] This calculation assumed that the energy difference between the excited singlet and triplet states is negligible. From these calculations we estimate the correlation energy to be $+0.32$ eV.

As was mentioned above, using a Green's-function local-density technique, Bar-Yam and Joannopoulos obtained a negative U for the dangling orbital in crystalline silicon. This result is in contrast with the DLTS and spin-resonance data[51] that indicate that the dangling orbital in amorphous silicon has a positive U of about 0.4 eV, as well as with the DLTS data on the P_b center that indicate a positive U of 0.6 eV. While the Bar-Yam–Joannopoulos result has prompted new defect models to account for the experimental observations,[52] we suggest that the lack of spin polarization in their calculation may explain the negative correlation energy. In his unrestricted X-α calculations on the P_b center, Cook encountered sizeable spin-polarization splittings.[37] In any case, a calculation of the correlation energies of some of the best understood dangling-bond-like defects in crystalline silicon, for which the correlation energies are known, would go far to establish confidence in the local-density results.

TABLE IV. Computed defect charges Q in the $+$, 0, and $-$ charge states for the Haldane-Anderson model (Ref. 29), and for MOPN. Q is in units of e.

	Q_+	Q_0	Q_-
HA	0.235	-0.013	-0.282
MOPN	0.436	0.122	-0.034

Controversy over the sign of the correlation energy should not overshadow the striking reduction from atomic values, ~10 eV, to tenths of an eV. The origin of this reduction is clearly illustrated in the Haldane-Anderson (HA) model Hamiltonian.[53] The interaction between the defect-atom orbitals and the band states of the unperturbed system leads to a delocalization of the defect wave function. Recently, Fowler and Elliott[29] have modified the HA Hamiltonian to include electronic and lattice polarization effects. This modification preserved the simple form of the HA Hamiltonian, while clarifying the approximations used in choosing the model parameters. They chose the dangling silicon orbital as the model system in their calculations. The degree of delocalization is measured by the net charge shifts on the defect atom arising from adding or subtracting an electron from the neutral defect. In Table IV we compare the Fowler-Elliott results with our own for cluster 6. We note that in our calculations the band states are replaced by the atomic orbitals on the other atoms. The agreement is striking, even though the finite cluster inherently limits the extent of the defect wave function. The charge shift between the positive and neutral charge states, 0.3e, is especially interesting when compared to the associated change in spin density on the defect atom, 0.8 spins. This clearly indicates the presence of large exchange effects.

V. CONCLUSION

In this paper we have presented a molecular-orbital study of the P_b center at the $\langle 111\rangle$ Si/SiO$_2$ interface. From our calculated spin-density matrix we have calculated hyperfine dyadics that agree in detail with Brower's observations.[3] It is gratifying that we can account for the superhyperfine shoulders as interactions on three second-nearest-neighbor silicon atoms. We also note the sensitivity of the principal hyperfine dyadic to relatively small displacements of the defect atom.

We have also studied the level structure of this defect in the positive, neutral, and negative charge states, where we have included electron-lattice interactions. Our estimates of the effective correlation energy agree well with the DLTS results of Johnson *et al.* Our results disagree with the recent calculation of Bar-Yam and Joannopoulos, who obtain a negative U, as well as a qualitatively different equilibrium geometry for the neutral state.[43] Finally, based on the response of both the singly and doubly occupied defect levels to compression, we predict the existence of a spin-dependent DLTS signal at high pressure.

ACKNOWLEDGMENTS

During the course of this work the author had helpful discussions with W. B. Fowler, N. M. Johnson, E. H. Poindexter, P. J. Caplan, and G. J. Gerardi. The comments of A. M. Stoneham about use of total-energy calculations for calculating defect electrical levels were very enlightening. The author thanks M. Cook and C. T. White for discussing their calculations prior to publication, and for useful critical comments during the preparation of this manuscript.

---

[1] Y. Nishi, Jpn. J. Appl. Phys. **10**, 52 (1971); Y. Nishi, K. Tanaka, and A. Ohwada, *ibid.* **11**, 85 (1972).

[2] A preliminary version of these calculations appeared in J. Electron. Mater. **14**, 491 (1984).

[3] K. L. Brower, Appl. Phys. Lett. **43**, 1111 (1983).

[4] N. M. Johnson, D. K. Biegelsen, M. D. Moyer, S. T. Chang, E. H. Poindexter, and P. J. Caplan, Appl. Phys. Lett. **43**, 563 (1983).

[5] R. C. Bingham, M. J. S. Dewar, and D. H. Lo, J. Am. Chem. Soc. **97**, 1285 (1975).

[6] P. Bischof, J. Am. Chem. Soc. **98**, 6844 (1976).

[7] A. H. Edwards and W. B. Fowler, J. Phys. Chem. Solids **46**, 841 (1985).

[8] M. H. White and J. R. Cricchi, IEEE Trans. Electron Devices **ED-19**, 1280 (1972).

[9] E. H. Nicollian and A. Goetzberger, Bell Syst. Tech. J. **46**, 1055 (1967).

[10] E. H. Nicollian and J. Brews, *MOS Physics and Technology* (Wiley, New York, 1982).

[11] P. V. Gray and D. M. Brown, Appl. Phys. Lett. **8**, 31 (1966).

[12] M. Kuhn, Solid State Electron. **13**, 873 (1970).

[13] N. M. Johnson, in *Proceedings of the Symposium of the Material Research Society*, edited by M.-A. Nicolet and N. W. Cheung (MRS, Pittsburg, 1986), Vol. 68, p. 75.

[14] E. H. Poindexter, G. J. Gerardi, M.-E. Rueckel, P. J. Caplan, N. M. Johnson, and D. K. Biegelsen, J. Appl. Phys. **56**, 2844 (1984).

[15] L. P. Trombetta (private communication).

[16] Spin resonance is not the only experimental tool with chemical sensitivity. Notably, Auger and x-ray photoelectron spectroscopy (XPS) has also been used to study the Si/SiO$_2$ interface, as well as the oxide layer. [For a review of XPS, see F. J. Grunthaner, P. J. Grunthaner, R. P. Vasquez, B. F. Lewis, J. Maserjian, and A. Madhukar, J. Vac. Sci. Technol. **16**, 1443 (1979), and references therein. For Auger spectroscopy of the interface, see C. R. Helms, W. E. Spicer, and N. M. Johnson, Solid State Commun. **25**, 673 (1978).] Because these spectroscopies do not require unpaired spins, they enjoy much wider potential use. They have, in fact, yielded very important insights into the structure of thermal oxides and into the morphology of the interface. However, because of the limited escape depth of photoelectrons or Auger electons, Auger and XPS are necessarily destructive techniques. Further, they yield only information about core levels, so that all information about the defect wave function and the position of the level in the gap is unavailable.

[17] A. G. Revesz and B. Goldstein, Surf. Sci. **14**, 361 (1969).

[18] A review of their most important spectroscopic results is found in E. H. Poindexter and P. J. Caplan, Prog. Surf. Sci. **14**, 201 (1983).

[19] K. L. Brower, Phys. Rev. B **26**, 6040 (1982).

[20] Recently, Stresmans has reported novel P_b resonances in samples oxidized at low pressures ($\sim 10^{-5}$ Torr). The orbitals associated with these signals point into the silicon substrate. These rsults are mentioned only for completeness and go beyond the scope of this paper. See A. Stesmans, Appl. Phys. Lett. **48**, 972 (1986).

[21] P. M. Lenahan and P. V. Dressenforfer, J. Appl. Phys. **55**, 3495 (1984).

[22] R. B. Laughlin, J. D. Joannopoulos, and D. J. Chadi, Phys. Rev. B **21**, 5733 (1980).

[23] K. L. Ngai and C. T. White, J. Appl. Phys. **52**, 320 (1981).

[24] W. A. Harrison, Bull. Am. Phys. Soc. **23**, 406 (1978).

[25] W. A. Harrison, Phys. Rev. B **8**, 4487 (1973).

[26] T. Sakurai and T. Sugano, J. Appl. Phys. **52**, 2889 (1981).

[27] A. S. Carrico, R. J. Elliott, and R. A. Barrio, Phys. Rev. B **34**, 872 (1986).

[28] A. H. Edwards (unpublished).

[29] W. B. Fowler and R. J. Elliott, Phys. Rev. B **34**, 5525 (1986).

[30] R. A. Barrio, R. J. Elliot, and A. S. Carrico, Phys. Rev. B **34**, 879 (1986).

[31] J. Bernholc, J. Electron. Mater. **14a**, 781 (1984).

[32] Y. Bar-Yam and J. D. Joannopoulos, Phys. Rev. Lett. **56**, 2203 (1986).

[33] While the Bernholc and the Bar-Yam–Joannopoulos calculations were intended to be relevant to amorphous silicon, they actually performed a calculation on a vacancy in crystalline silicon decorated with three hydrogen atoms.

[34] P. W. Anderson, Phys. Rev. Lett. **34**, 953 (1975).

[35] A. Redondo, W. A. Goddard, and T. C. McGill, J. Vac. Sci. Technol. **21**, 649 (1982).

[36] A. Redondo, W. A. Goddard, T. C. McGill, and T. C. Surratt, Solid State Commun. **20**, 733 (1976).

[37] M. Cook and C. T. White, Phys. Rev. Lett. **59**, 1741 (1987).

[38] R. Fletcher and M. J. D. Powell, Comput. J. **6**, 163 (1963); W. C. Davidon, *ibid.* **10**, 406 (1968).

[39] A. Abragam and B. Bleaney, *Electron Paramagnetic Resonance of Transition Metals* (Clarendon, Oxford, 1970).

[40] GAUSSIAN-82 is an *ab initio* molecular-orbital program obtained from Carnegie-Mellon University.

[41] R. E. Watson, Phys. Rev. **111**, 1108 (1958).

[42] A. Mainwood, J. Phys. C **11**, 2703 (1978).

[43] In the Bar-Yan—Joannopoulos calculation, the defect atom moves ~ 0.1 Å *out* of the plane of its three nearest-neighbor atoms, contrary to all other calculated results and to simple chemical intuition.

[44] Valence-band spin polarization has been discussed in H. Katayama-Yoshida and K. Shindo, J. Electron. Mater. **14a**,

73 (1984).

[45] Chen and Lang have performed spin-dependent DLTS on $\langle 111 \rangle$ MOS samples [M. C. Chen and D. V. Lang, Phys. Rev. Lett. **51**, 427 (1983)]. From the existence of a very weak spin-dependent effect, they inferred that the true effective correlation energy was ~ 0.1 eV. In their explanation for this effect, they argued that it was due to a spin-dependent modulation of the total charge, rather than of the capture rate. It is interesting that the model to which they referred, D. Kaplan, I. Solomon, and N. F. Mott, J. Phys. (Paris) Lett. **39**, L51 (1978), was in fact a rate-modulation model.

[46] A. Jayaraman, Rev. Mod. Phys. **55**, 65 (1983).

[47] M. F. Li, P. Y. Yu, E. R. Weber, and W. Hanson (unpublished).

[48] I. Spain (private communication).

[49] R. S. Mulliken, in *Quantum Theory of Atoms, Molecules, and the Solid State,* edited by P. O. Lowdin (Academic, New York, 1966), p. 231.

[50] This band gap is significantly lower than the MNDO or MINDO/3 estimates, ~ 2.0 eV, obtained with the half-electron approximation. This probably reflects the configuration interaction inherent in the unrestricted Hartree-Fock formalism.

[51] D. K. Biegelsen and M. Stutzmann, Phys. Rev. B **33**, 3006 (1986).

[52] S. T. Pantelides, Phys. Rev. Lett. **57**, 2979 (1986).

[53] F. D. M. Haldane and P. W. Anderson, Phys. Rev. B **13**, 2553 (1976).